City Research Online

City, University of London Institutional Repository

Journal of Comparative Physiology A

The arm skeleton and shoulder girdle of Falco peregrinus, Falco tinnunculus, Accipiter nisus, and Columba livia domestica
--Manuscript Draft--

Manuscript Number:	JCPA-D-18-00015
Full Title:	The arm skeleton and shoulder girdle of Falco peregrinus, Falco tinnunculus, Accipiter nisus, and Columba livia domestica
Article Type:	Original Paper

Abstract:	During a high-speed dive peregrine falcons (Falco peregrinus) can reach a flight velocity of up to 320 kmh-1. In consequence the bones of the wings and the shoulder girdle of peregrine falcons most likely experience large mechanical forces. We investigated the bones of the arm skeleton and the shoulder girdle of peregrine falcons. For comparison, we also investigated the comparable bones in European kestrels (Falco tinnunculus), sparrow hawks (Accipiter nisus) and pigeons (Columba livia domestica). The normalized bone mass of the entire arm skeleton and the shoulder girdle (coracoid, scapula, furcula) was significantly higher in F. peregrinus than in the other three species investigated. The midshaft cross-section of the humerus of F.peregrinus had the highest specific bending stiffness per body mass and the highest second moment of area. The mineral densities of the humerus, radius, ulna, and sternum were highest in F.peregrinus, indicating again a larger overall stability of these bones. Furthermore, the bones of the arm and shoulder were strongest in peregrine falcons. Computational fluid dynamics simulations suggest, that the forces that pull on the wings of a peregrine can reach up to three times the falcon's body mass at a stoop velocity of 80 ms-1.

Corresponding Author:	Horst Bleckmann Universität Bonn Bonn, GERMANY
Corresponding Author Secondary Information:	
Corresponding Author's Institution:	Universität Bonn
Corresponding Author's Secondary Institution:	
First Author:	Horst Bleckmann
First Author Secondary Information:	
Order of Authors:	Horst Bleckmann
	Anke Schmitz
	Nele Ondreka
	Julia Poleschinski
	Dominik Fischer
	Adrian Klein
	Helmut Schmitz
	Christoph Brücker
Order of Authors Secondary Information:	

Author Comments:	We would like to publish this MS about peregrine falcons in JCP. The MS is about numerical simulations of the forces acting on the wings of a diving

	peregrine and morphological adaptations regarding the wing bones.
Suggested Reviewers:	Stanislav Gorb, PhD Professor C4 sgorb@zoologie.uni-kiel.de Gorb is a specialist in animal morphology and morphological adaptations
	Reinhard Blickhan, PhD Prof. em. Reinhard.blickhan@uni-jena.de Blickhan is a specialist in biomechanics and in fluid dynamics

The arm skeleton and shoulder girdle of *Falco peregrinus*, *Falco tinnunculus*, *Accipiter nisus*, and *Columba livia domestica*

Anke Schmitz*[1], Nele Ondreka[2], Julia Poleschinski[2], Dominik Fischer[3],

Helmut Schmitz[1], Adrian Klein[1], Horst Bleckmann[1], Christoph Bruecker[4]

[1] Institute of Zoology, Rheinische Friedrich-Wilhelms-University Bonn, Bonn, Germany, [2] Small Animal Clinic, Department of Veterinary Clinical Sciences, Justus Liebig University Giessen, Giessen, Germany, [3] Clinic for Birds, Reptiles, Amphibians and Fish, Department of Veterinary Clinical Sciences, Justus Liebig University Giessen, Giessen, Germany , [4] School of Mathematics, Computer Science and Aeronautics, City University London, UK

*corresponding author:

Dr. Anke Schmitz

Institute for Zoology

Rheinische Friedrich-Wilhelms-University Bonn

Poppelsdorfer Schloss

53115 Bonn, Germany

Email: ankeschmitz@uni-bonn.de

Abbreviations

BM	Body mass
BMD	Bone mineral density
CA	Area of compact bone in a cross section
CFD	Computation fluid dynamics
E	Youngs modulus
HA	Hydroxyapatite
HU	Hounsfield unit
I	Second moment of area
J	Polar moment of area

Abstract

During a high-speed dive peregrine falcons (*Falco peregrinus*) can reach a flight velocity of up to 320 kmh[-1]. In consequence the bones of the wings and the shoulder girdle of peregrine falcons most likely experience large mechanical forces. We investigated the bones of the arm skeleton and the shoulder girdle of peregrine falcons. For comparison, we also investigated the comparable bones in European kestrels (*Falco tinnunculus*), sparrow hawks (*Accipiter nisus*) and pigeons (*Columba livia domestica*). The normalized bone mass of the entire arm skeleton and the shoulder girdle (coracoid, scapula, furcula) was significantly higher in *F. peregrinus* than in the other three species investigated. The midshaft cross-section of the humerus of *F.peregrinus* had the highest specific bending stiffness per body mass and the highest second moment of area. The mineral densities of the humerus, radius, ulna, and sternum were highest in *F.peregrinus*, indicating again a larger overall stability of these bones. Furthermore, the bones of the arm and shoulder were strongest in peregrine falcons. Computational fluid dynamics simulations suggest, that the forces that pull on the wings of a peregrine can reach up to three times the falcon's body mass at a stoop velocity of 80 ms^{-1}.

Introduction

The peregrine falcon (*Falco peregrinus*) is the world's fastest bird. While attacking its bird prey in midair (Mebs and Schmidt 2005) a diving peregrine can reach velocities of up to 320 kmh[-1] (Tucker and Parrott 1970; Orton 1975; Tucker 1990; Savage 1992; Clark 1995; Peter and Kestenholz 1998; Franklin 1999, 2011). To learn more about the flight of peregrines, wing contours and flight trajectories of diving peregrines were investigated by Ponitz et al. (2014a, b). These investigations suggest that during a dive, but also while pulling out of a dive, the arm skeleton and the wings and tail feathers of *F.peregrinus* are exposed to large mechanical forces (Ponitz et al. 2014a). To uncover possible adaptations that allow peregrines to cope with these forces, Schmitz et al. (2015) studied the morphology and material properties of the wing and tail feathers of *F. peregrinus* (primary 10, alula one, central tail feather). For comparison Schmitz et al. (2015) also investigated the corresponding feathers in sparrow hawks (*Accipiter nisus*), European kestrels (*Falco tinnunculus*) and pigeons (*Columba livia domestica*). The latter three

species were chosen because they differ markedly in flight style but do not reach the high flight velocities of a diving peregrine. According to Schmitz et al. (2015) the tail feathers of *F. peregrinus* are more stable than the corresponding feathers of the other three bird species.

During a dive, peregrines alter the shape of their wings; while accelerating, they move them closer and closer to their body (Franklin 1999). At top velocities they build a wrap dive vacuum pack, *i.e*. the wings are completely folded against the elongated body (Seitz 1999). Peregrines are not only extremely fast flyers but also maintain a remarkable maneuverability at high flight speeds. For instance, during courtship they often turn sharply from a fast vertical dive into a steep climb (H.Bleckmann, pers. observation).

Out of the four bird species investigated in the present study, *C. livia domestica* is the most sustained flyer (Heinzel et al. 1992) In this species bones show no striking morphological adaptations (Pennycuick 1968a; Dial 1992; Bachmann et al. 2007; Berg and Biewener 2010). Since the forces acting on the wings of a peregrine falcon during a dive can hardly be measured directly, we used finite element analysis to calculate these forces. Our calculations indicate that up to 350 g may pull on the wings of a peregrine diving with a velocity of 80ms^{-1} (288 kmh^{-1}). Due to the expected high forces experienced by the wings of a diving peregrine (or while pulling-out of a dive), the wing and shoulder bones should be significantly stronger in peregrines than in other bird species (Norberg 1981, 1985; Selker and Carter 1989). We tested this hypothesis by investigating the bones of the arm skeleton and the shoulder girdle of *F. peregrinus*. For comparison we also studied the comparable bones in *F. tinnunculus*, *A. nisus* and *C. livia domestica*.

Material and Methods

Animals

Four bird species were investigated: *F. peregrinus* (Tunstall 1771), *F. tinnunculus* (Linneus 1758), *A. nisus* (Linneus 1758) and captive bred *C. livia domestica* (Gmelin 1789). In all species, four males and four females were investigated. Mean body masses were 546 g ± 58 (male *F. peregrinus*) and 849 g ± 34 (female *F. peregrinus*), respectively. The corresponding values for *F. tinnunculus* and *A.nisus* were 167 g ± 12 and 218 g ± 11 (males) and 165 g ± 2 and 224 g ± 16 (females). Mean body mass of *C.livia domestica* was 479 g ± 16, values for males and females were not significantly different.

Animals were provided by Walter Bednarek (two *F. tinnunculus*; CitesNr. DE-COE121306201, two *A. nisus*; DE-COE121206202 and one *F. peregrinus*; DE-COE080818171); another *F. peregrinus* was supplied by Daniel Müller (DE-HF98050800001). Carcasses of six *F. peregrinus*, six *F. tinnunculus*, six *A. nisus* and eight *C. livia domestica* were provided by the Clinic for Birds, Reptiles, Amphibians and Fish at the Justus-Liebig-University of Giessen, Giessen, Germany in cooperation with the Society to Support Avian Medicine in Giessen (Verein zur Förderung der Vogelmedizin in Gießen e.V.). All animals included in our study were submitted by private persons immediately after being found or by veterinarians and rehabilitation centers in the first 48 hours upon admission. Birds which had been kept in captivity for more than two days were excluded from the study. All individuals were clinically examined including radiographic examination in latero-lateral and ventro-dorsal view. Dead animal were inspected during routine necropsy. Therefore, only injured animals with a presumptive acute cause of injury were included in the study without findings of an underlying subacute or chronic course of disease. Examination (preparation of the carcasses, detailed investigation of muscles and bones) of these birds was authorized by the Regierungspräsidium Giessen, Dezernat 53.2. No bird was killed for our study. Therefore, no permits for animal experiments were needed. All animals were stored at -18°C and thawed 16-24 hours before dissection. Animals were kept in a freezer for less than six months before investigation. All animals of a given species and sex had a comparable body mass (BM); their muscles did not show any signs of autolysis. From each animal BM and body length were obtained. Feathers and skin were removed unilaterally. Four individuals per species were fixed in 4% formaldehyde in phosphate buffer for two weeks. After fixation, animals were stored in a solution that contained 0.5% formaldehyde. Four individuals from each species were prepared immediately after thawing. Freezing of specimens prior to investigation may increase the strength of the bones slightly but does not change any other bone properties (Turner and Burr 1993). All bone mineral density (BMD) measurements (see below) were performed on individuals prior to fixation.

Bones

Bone integrity was verified radiographically before further analysis using a high-frequency digital diagnostic x-ray unit (Gierth HF 400A, GIERTH X-Ray international GmbH, Riesa, Germany). Only one side of the body from each animal was used for analysing the arm skeleton and the thorax. All muscles were removed and the bones were cleaned manually. Finally, bones were air-dried and the length of the arm skeleton was measured from the shoulder joint (reference point middle of epiphysis) to the tip of the *Digitus major*. Finally, data were related to BM. The

masses of the arm and shoulder skeleton (masses per BM) were determined after rewetting the bone pieces in a physiological saline solution (0.9% NaCl = 9 g NaCl/L) for 24 h, since wet bones are more similar to the bones of a living animal than dry bones (Zysset et al. 1999). The shoulder skeleton consisted of the coracoid, the scapula and the halved furcula. Measurements were conducted on eight specimens of each species.

The midshaft cross-sections of the humeri (Fig. 1) were chosen as focal point of our analyses because the humerus has to cope with the highest bending stresses (Biewener and Taylor 1986a, b). For our investigations the humeri of four specimens per species were immersed in a physiological saline solution for 24 hours. From the midpoint of the humeri, 2-3 mm thick slices were cut off with a coping saw. Bone pieces were air-dried, embedded in epoxy resin (Toolcraft, epoxy resin L and hardener L), and polished with a diamond point. The trimmed bone areas were used for the determination of the second moment of area (I) and the Young's modulus (E). I was determined by point counting of the trimmed bone areas (Purslow and Vincent 1978; Schmitz et al. 2015). Drying and rewetting had no effect on I as the bone pieces were embedded in Epon. For the determination of I, the bones were bend in dorso-ventral (I_{dv}), lateral (I_{lat}) and diagonal (I_{diag}) direction (Fig. 1e). Finally, I was normalized to the BM of the respective animal. This allowed estimating the resistance of a bone to bending loads (Boresi and Schmidt 2002; Simons et al. 2011; Brassey et al. 2013).

For the determination of the Youngs modulus, samples were rewetted as the dry status of bones is far from the physiological condition of the bones of a living animal (Zysset et al. 1999). Rewetting was done 2 hours prior to measurements. With a nanoindenter (*Hysitron Triboscope, D3100*), 72 indents were performed per trimmed bone area using a Berkovich diamond tip with a load of 5000 µN. This load caused a contact depth of about 400 nm. The specific bending stiffness M is:

$$M = (E * I) * d^{-1} \qquad\qquad (1)$$

with E = Young's modulus (Nm^{-2}), I = second moment of area (m^4) and d = sample width (m). Hardness and E were calculated with the Hysitron software from the unloading portions of the load-displacement curves following a procedure given by Oliver and Pharr (1992). M was finally normalized to the BM of the respective bird.

The polar moment of area J was calculated according to:

$$J = I_{lat} + I_{dv} \tag{2}$$

with I_{lat} and I_{dv} being orthogonal to each other (Boresi and Schmidt 2002; Simons et al. 2011), J - normalized to BM - is a measure for the resistance of a bone to torsion (Brassey et al. 2013).

The cortical area (CA) of compact bone in a given cross section (Fig. 1), determined by point counting, was used to estimate the resistance of a bone to compressional loading (Boresi and Schmidt 2002; Simons et al. 2011; Brassey et al. 2013). The thickness of the cortex can be described by the dimensionless parameter K, which is the inner diameter divided by the outer diameter of a bone cross section (Selker and Carter 1989; Simons et al. 2011). Measurements were obtained from four specimens (2 males and 2 females) of each species. Finally CA was normalized to BM.

According to Currey (2002), the maximum stress that BM can exert on the bones of a given bird species is proportional to $BM^{1/3}$. Moreover, the force at which a bone will break (F) is proportional to $BM^{2/3}$.

Bone mineral density

Bone mineral density (BMD) measurements were performed on freshly thawed birds and after computer tomographic scanning. Bones and muscles were separated and bones were prepared as described above. Computed tomographic scans were obtained with a 3rd generation 16-slice helical scanner (PHILIPS Brilliance, Fig. 2) using a standard protocol: 0.7mm slice thickness, 140kV, 200mA. Three specimens per species were investigated. System calibration was done with a customized liquid dipotassium hydrogenphosphate phantom consisting of five cylindrical tubes with permanent reference densities (distilled water as well as hydrogen-phosphate diluted in distilled water: 1:100, 1:200, 1:400, 1:800), acting as bone mineral and water equivalent. The phantom was placed on the animal during the scan (Kalender et al. 1995; Cann 1988) and a calibration curve was prepared for each scan. BMD was measured within stacks of manually drawn regions of interest and within standardized regions of the long bones covering a predefined percentage of the entire bone length. For the long bones (humerus, radius, ulna, coracoid and clavicula) a mid-diaphyseal stack covering 10% of the entire bone length and a proximal and distal metaphyseal stack sparing the former physis covering 5% of the entire bone length,

respectively, were obtained. For the scapula, 10% of the entire bone length was obtained in the region of the neck and at its widest cranio-caudal dimension. Mean, range and standard deviation (SD) of the Hounsfield units (HU) within the regions of interest were used for analysis. BMD was determined according to phantom based quantitative computer tomography using a conventional multislice computer tomograph scanner and a customized K_2HPO_4 phantom. Quantitative computer tomography is an established method to assess BMD and relative risk of osteoporotic fracture in people and does not implement added filtration. To address the systematic error potentially introduced by the polychromatic nature of the x-ray beam and beam hardening effects, strict standardization of the study set up was observed (Ruegsegger et al. 1976; Cann 1985; Cann et al. 1985). Moreover, the influence of beam hardening on BMD is assumed to be small and negligible in diaphyseal areas of the bone, as these areas are composed of a thin cortex and an "empty" pneumatized medullary cavity only. BMD measurements comprised cortical bone, blood, fatty tissue, and pneumatized regions of the medullary cavity. BMD values are expressed as equivalent densities in milligrams of K_2HPO_4 per millilitre of bone tissue (HA, mg cm^{-3}) using a calibration phantom and a linear regression model.

Computation Fluid Dynamics

We calculated the forces acting on the wings of a diving peregrine using computational fluid dynamics (CFD), from which the pressure distribution and shear stresses along the body and wing contours can be derived. The present study builds on previous detailed field studies of life bird and wind-tunnel experiments of realistic models of peregrine falcons (Ponitz et al. 2014a, b), which is the base for the 3D geometry of the wing and body shape used herein, i.e. the cupped wing configuration (see Ponitz et al. 2014a). The present method follows a procedure desribed in Ponitz et al. (2014a). The three-dimensional CAD model of the falcon was transferred into a computational unstructured grid using a grid generation tool ICEM CFD 14.5 (ANSYS, Inc., Canonsburg, PA, USA). The computational domain includes the inflow region, the falcon region, and the downstream wake region of the flow. Special attention was paid to the meshing of the falcon. Refinements toward near-wall regions were taken into consideration. The grid consists in total of 6.5 million unstructured tetrahedron cells and 1.5 million prism cells on the falcon surface. A mesh independency check for the results of lift and drag coefficients was done for up to 10 million cells. Simulation stability was investigated in respect to different grid parameters and following settings leads to stable results: The height of the first prisms layer on the falcon surface was set to 0.1 mm with a growth factor of 1.1 for the following layer perpendicular to the wall and a total number of 10 layers. For these simulation parameters the numerical flow

simulations delivered stable values which furthermore matched the experimental results of lift and drag forces obtained from the wind-tunnel tests (see Ponitz et al. 2014a, b). The numerical flow simulation was performed using the open source CFD software OpenFOAM (OpenCFD Ltd., Bracknell, UK). The code numerically solves the conservation equations of mass and momentum by means of a finite volume approach (https://www.openfoam.com/documentation/tutorial-guide/):

$$\frac{\partial}{\partial x_i}\left(u_i\right)=0 \quad , \quad \frac{\partial}{\partial x_i}\left(u_j\, u_i\right)=-\frac{1}{\rho}\frac{\partial p}{\partial x_i}+\frac{1}{\rho}\frac{\partial \tau_{ij}}{\partial x_j} \tag{3}$$

with p = pressure, u = velocity vector, x = Cartesian coordinate system, and ij = stress tensor in Einstein notation. The calculation of the resulting forces F on the body segments were done by integrating the pressure over the outer surface exposed to wind.

$$\vec{F} = -\oiint\left(p\cdot\vec{n}\right)dA \tag{4}$$

This excluded the part of the surface where the segment is separated from the body.

In our simulations air was treated as a single-phase, incompressible (0.07 Ma), isothermal (20˚C) Newtonian fluid with constant density (1.189 kgm^{-3}) and viscosity (18.232 $\times10^{-6}$ Pas). Three different stoop velocities were simulated, beginning with 22.5 ms^{-1}, as observed in our experiments on a dam wall (Ponitz et al. 2014a). We then increased the stoop speed in the simulations to 40 ms^{-1} and to a maximum of 80 ms^{-1}, a speed that diving peregrines most likely can reach (Franklin 1999, 2011; Orton 1975; Tucker and Parrott 1970). The Reynolds number Re, based on the body length of a peregrine (400 mm), is for all three cases $> 5\times10^5$. Therefore, turbulent flow was taken into account by a Reynolds averaged approach (Spalart-Almaras turbulence model). The no slip boundary condition was applied to the body surface. For calculating the forces acting on the wings, we segmented the body in 4 parts: the two wings, the tail and the center body. Integration of the pressure and shear-stress along the surface segments then provide the caudal, dorsal, and distal forces on the wing. In aerodynamic notation these forces on the wing correspond to the drag, the lift force and the side-force of an aerofoil.

The wing configuration chosen was the "cupped wing configuration", one which a peregrine adapts late in a stoop as it starts to pull-out (Ponitz et al. 2014a, b). The formulation "cupped wings" was introduced by Tucker and Parrott (1970) to describe the shape of the downward tilted tips of the wing which is a typical falcon shape during a dive. In the cupped wing formation, air can enter the space between the wing and the body which affects the lateral forces on the wings. The transition to pull-out is when we expect the largest forces acting on the body and the wing as this is the moment of change from a straight flight path into a curved one. This requires an increase in lift forces to overcome the centrifugal forces at such high speeds.

Statistics

Mean values and standard deviations (SD) were calculated. Differences between species were compared using SPSS (IBM, version 22). Distribution of the data was tested with a one-sample Kolmogorov-Smirnov test. One-way analysis of variance (ANOVA) with Bonferroni test as post-hoc evaluation was used to compare mean values of different species if values were normally distributed. If data did not follow a Student's t-distribution, a Mann-Whitney-U test was applied. If not otherwise stated significance level was P<0.05. In most figures significant differences are only shown for *F. peregrinus*.

Results

Bones

Normalized to body mass (BM), *F. peregrinus* and *C. livia domestica* had the shortest arm skeleton (Fig. 3a). In *F. peregrinus* the mass of the arm and shoulder skeleton, also normalized to BM, was higher than in the other three species (Fig. 3 b, c). *C. livia domestica* had the largest pectoral muscles (not shown), but a relatively light weight arm and shoulder skeleton. The Young's modulus E of the humeri (Table 1) was highest in *F. peregrinus,* followed by *F. tinnunculus, A. nisus* and *C. livia domestica.* The maximum and minimum of I was greatest in *F. peregrinus* (Table 1). If normalized to BM, I was greatest in *F. peregrinus* for all bending directions applied (Fig. 4a). The calculated M value, if normalized to body mass, was also higher in *F. peregrinus* than in the other three bird species (Fig. 4b). In the normalized data sex differences were not found.

The maximum stress that the body mass can exert on the bones of a bird is proportional to body mass$^{1/3}$. The force F is proportional to body mass$^{2/3}$ (Currey 2002). Using these relations, the

maximum stress to which the bones will be exposed is 1.2 times larger in *F. peregrinus* than in *C. livia domestica* (males 1.04, females 1.2) and 1.6 times larger in *F. peregrinus* than in *F. tinnunculus* and *A. nisus* (1.48 and 1.57). Moreover, the force at which the humeri of *F. peregrinus* will break is 1.3 times larger in *F. peregrinus* than in *C. livia domestica* (males 1.08, females 1.44) and 2.3 times larger in *F. peregrinus* than in *A. nisus* and *F. tinnunculus*. (2.18 and 2.45).

The calculated J value and CA were greatest in *F. peregrinus* (Figs. 5, 6a). If normalized to body mass, differences between raptor species vanished, but the difference to *C. livia* domestica remained (Fig. 6e). All species possessed thin-walled humeri (as indicated by the K-values in Fig. 7). Humeri of *F. peregrinus* had the lowest K-value, i.e. the humeri of peregrines had the thickest walls. However, only the difference to *C. livia domestica* was significant.

BMD, expressed as the amount of hydroxyapatite (Cann 1988; Damilakis et al. 2007), was highest in *F. peregrinus* (humerus, radius, ulna, and sternum) (Fig. 8b). The scapula and furcula of *C. livia domestica* revealed the highest values, followed by the values of *F. peregrinus*. The coracoid had a similar HA-value in all species (Fig. 8b). The calculated HA-values showed the same relationships as the values on the Hounsfield scale (HU). HU was used to calculate the statistics, as shown in Fig. 8a.

Forces acting on the wings

Our morphological data show that the humerus, ulna, radius and sternum of peregrine falcons are extraordinarily strong (Figs. 4, 5, 6, and 8). This supports our working hypothesis that the wings of a diving peregrine are exposed to extraordinary large forces. To estimate these forces we performed CFD simulations. Figure 9 shows the side and front view of the "cupped wings" configuration of a diving peregrine. This configuration was used for our calculations (Fig. 10). The initial assumed stoop speed was 22.5ms^{-1}, the angle of incidence was 5°. Aerodynamic conditions were derived from high-resolution tracking and imaging of life birds (Ponitz et al. 2014a). In Fig. 10, the segment of the wing that was used for the integration of the forces is coloured in blue. Forces are given in a body-related coordinate system. Figure 10 shows that the distal force acting on the wings pull the cupped part of the wings away from the body. This force is of the same order of magnitude as the dorsal force, which corresponds to the lift force acting on the wing.

Calculations for three diving speeds show that the forces acting on the wings of a diving peregrine scale proportional to the square of diving velocity (Fig. 11). For an adult peregrine falcon (assumed mass 500 g) and a diving velocity of 80 m/s (288 km/h) the flight muscles of the falcon must develop a force of -11.5 Newton in dorsal direction and -9 Newton in distal direction (the negative sign hints that the muscle forces are pointing towards the body axis to counter-act the aerodynamic forces). Thus, compared to the weight of a peregrine falcon the forces that the wings may experience are in total about 3-times higher.

Discussion

Our results are consistent with the data reported for other bird species. The second moment of area I in *Larus californicus* (California gull) of the humerus varies between 1 and 40 mm^4 (BM of the animals was 40 to 700 g) (Carrier and Leon 1990). This agrees well with our values for *C. livia domestica* (body mass about 450 g, I=23-38 mm^4). To our knowledge the Young' modulus of the humerus has been measured by nanoindentation for two species of penguins; the values obtained are 19.5-22.1 GPa (Currey 1988). In volant birds, the thickness of the cortices (K-values) of the humeri varies between 0.68 and 0.86: the K-value for the humerus of *C. livia domestica* is 0.83 (Currey and Alexander 1985). These values are similar to our value for *F. peregrinus* (0.85).

Most previous studies that assessed the mechanical properties of bones used a Berkovich tip and the Oliver and Pharr calculation (Oliver and Pharr 1992). There is some evidence that E of a bone can be overestimated by using this method (Rodriguez-Florez et al. 2013). Bones are anisotropic and viscoelastic. To obtain realistic values with a Berkovich tip (Oliver and Pharr 1992), the material under investigation must be isotropic and elasto-plastic. To get realistic values we corrected for viscoelastic effects as described by Tang and Ngang (2004) and Tang et al. (2007). Based on these studies, Ngan (University of Hong Kong, Department of Mechanical Engineering) calculated, that our data must be multiplied with the correction factor 0.78.

Bones

A long bone rarely fractures in a living animal due to pure axial loads (Carter and Spengler 1982). Most fractures are caused by stresses created by bending and torsion (Rubin and Lanyon 1982; Biewener et al. 1983; Biewener and Taylor 1986a, b), forces that especially affect the humerus and the forearm of a bird (Bou et al. 1991; Biewener and Dial 1995). The resistance against bending and torsion is higher in thin walled bones with a large diameter (de Margerie et

al. 2005). For bending and torsional loading, the force that is required to fracture a bone is proportional to $BM^{2/3}$ (Selker and Carter 1989; Currey 2002). In the bird species investigated in this study, forces that may lead to bone fracture were more than twice as high in *F. peregrinus* than in *A. nisus* and *F. tinnunculus* and 1.3 times higher than in *C. livia domestica*. The large body mass of the peregrine falcon is one factor that requires solid bones, i.e. bones that resist fractures. A second factor are probably the forces to which the wing bones of a peregrine are exposed during a high-speed dive (Figs. 10, 11). The humerus, radius and ulna of peregrines probably resist these loads more effectively than the corresponding bones of the other bird species investigated.

Bone geometry is the primary variable that determines bone strength (Selker and Carter 1989). The midshaft cross-section of long bones can resist the highest bending stresses (Biewener and Taylor 1986; Beer et al. 2006). A circular structure with a large diameter and a thin cortex (e.g. the humeri of alate birds) has a higher I value and a greater resistance against bending and especially against torsion than a structure with a small diameter and a thick cortex (Biewener 1982; Alexander 1983; Currey and Alexander 1985; Swartz et al. 1992; Swartz 1997; de Margerie et al. 2005; Habib and Ruff 2008; Dumont 2010). All humeri of the bird species investigated in the present study had thin cortices and a high K-value. This indicates a potential bending in multiple planes and/or high amounts of torsion in the humerus (Habib and Ruff 2008). The relatively low K-value of *F. peregrinus* coincides with the higher mass and a higher M value of its arm skeleton. Even though the difference to the other species is small it may indicate an adaptation to fast flight manoeuvres.

Circular humeri are equally resistant against bending in all directions, whereas elliptical humeri have the highest resistance to bending in the direction of the largest cross section (Simons et al. 2011). The cross sections of the humeri of the bird species investigated in this study were round or elliptical. Because of the high second moments of area I and polar moments of area J in *F. peregrinus*, the bending loads and the resistance to torsion were higher in *F. peregrinus* than in the other three species (Figs. 4, 5). If normalized to body mass (Fig. 4a), the humeri of *F. peregrinus* still have the highest I value in the bending directions tested. The round shaped cross section of the humerus together with the high I and J values might ascertain that this bone can resist high forces from all directions.

The resistance to compressional loads (CA) was higher in *F. peregrinus* than in the other species investigated. However, if normalized to body mass, values no longer were significantly different from the value of *C. livia domestica* (Fig. 6b). CA most likely is not an important parameter for coping with the high forces during a dive. BMD derived from quantitative CT as measured by dipotassium hydrogenphosphate equivalents per volume unit reflect bone strength and correlates with the relative risk of fracture (Marshall et al. 1996). Besides the higher M-value of the humeri, BMD-values of the entire wing bones also indicate that the wing bones of *F. peregrinus* are more stable than the wing bones of the other bird species investigated. In *F. peregrinus*, the scapula and furcula are less mineralised than in *C. livia domestica*. The high mineralization of the scapula and furcula of *C. livia domestica* most likely is an adaptation to the forces produced by the great breast muscles (especially the *M. pectoralis*) of pigeons.

Forces acting on the wings

Our CFD simulations show that the aerodynamic lift force component acting on the wings (in dorsal direction) is the highest, followed by the side-force component (distal) that tries to pull the cupped part of the wings away from the body. Both are of the same order of magnitude, while the drag force component (caudal) is considerably lower. The flight muscles of a diving peregrine have to counter-act these aerodynamic forces to keep the wings close to the body. The calculations for three diving speeds show that the forces acting on the wings scale proportional to the square of diving velocity. The flight muscles of a peregrine falcon of 500 g weight and an assumed diving velocity of 80 ms^{-1} (288 kmh^{-1}) must develop a force of -11.5 Newton in dorsal direction and -9 Newton in distal direction (the negative sign indicates that the muscle forces are pointing towards the body axis to counter-act the aerodynamic forces). Thus, compared to the weight of the falcon the forces that the wings experience at the end of a dive are about 3-times higher. Note that these aerodynamic forces may even be larger if the bird is going into a higher angle of incidence during pull-out. This probably explains while the bones of the arm and shoulder are so strong in peregrine falcons.

The present study shows, that the forces acting on the wings of a diving bird largely depend on flight velocity (Fig. 11). Kestrels dive after a windhovering bout to stoop on their ground dwelling prey, however, the estimated height from which they start a dive usually is below 60 meters (personal observation). From this height even a diving peregrine falcon does not reach speeds larger than 60 kmh^{-1} (Ponitz et al. 2014a). Thus the velocity of a diving kestrel is far less than the velocity of a diving peregrine falcon. Consequently, the maximal forces acting on the

wings of a diving kestrel are much smaller than the forces acting on the wings of a diving peregrine. During courtship or prior to prey capture many eagles also dive. To our knowledge the maximum diving speed of eagles has, however, never been measured. So far, no bird known can match the flying speed of a peregrine falcon in its hunting dive. Further investigations should analyse the bone architecture of peregrine falcons in more detail as the ultrastructure may also be crucial in determining the biomechanical properties of bones adapted to potentially extreme loads.

References

Alexander RM (1983) Animal mechanics. Oxford, Blackwell Scientific Publications.

Bachmann T, Klän S, Klän S, Baumgartner W, Klaas M, Schröder W, Wagner H (2007) Morphometric characterisation of wing feathers of the barn owl *Tyto alba pratincola* and the pigeon *Columba livia domestic*. Front Zool 4:23-38.

Beer F, Johnston ER, DeWolf JT, Mazurek DF (2006). Mechanics of Materials. McGraw-Hill Science.

Berg AM, Biewener AA (2010) Wing and body kinematics of takeoff and landing flight in the pigeon (*Columba livia*). J Exp Biol 213:1651-1658

Biewener AA (1982) Bone strength in small mammals and bipedal birds - do safety factors change with body size? J Exp Biol 98:289-301

Biewener AA, Dial KP (1995) In vivo strain in the humerus of pigeons (*Columba livia*) during flight. J Morphol 225:61-75

Biewener AA, Taylor CR (1986a) Bone strain: a determinant of gait and speed? J Exp Biol 123: 383-400

Biewener AA, Taylor CR (1986b) Bone stress - a determinant of top speed. J Biomech 19:473-473

Biewener AA, Thomason J, Lanyon LE (1983) Mechanics of locomotion and jumping in the forelimb of the horse (*Equus*): in vivo stress developed in the radius and metacarpus. J Zool 201:67-82

Boresi AP, Schmidt RJ (2002) Advanced Mechanics of Materials. New York, John Wiley & Sons, pp 1-700

Bou J, Olmos M, Casinos A (1991) Strengths of the limb bones of birds and small mammals in bending and twisting. Annales Des Sciences Naturelles-Zoologie Et Biologie Animale 12:197-207

Brassey CA, Kitchener AC, Withers PJ, Manning PL, Sellers WI (2013) The role of cross-sectional geometry, curvature, and limb posture in maintaining equal safety factors: a computed tomography study. Anatomical Record-Advances Integrative Anat and Evol Biol 296: 395-413

Cann CE (1988) Quantitative CT for determination of bone mineral density - a review. RSNA Radiology 166:509-522

Cann CE, Genant HK, Kolb FO, Ettinger B (1985) Quantitative computed tomography for prediction of vertebral fracture risk. Bone 6:1-7

Carrier D, Leon LR (1990) Skeletal growth and function in the california gull (*Larus californicus*). J Zool 222:375-389

Carter DR, Spengler DM (1982). Biomechanics of fracture. Philadelphia, WB Saunders.

Clark WS (1995) How fast is the fastest bird? Wild Bird 9:42-43

Currey JD (1988) The effect of porosity and mineral-content on the Young's modulus of elasticity of compact bone. J Biomechan 21:131-139

Currey JD (2002). Bones. Structure and Mechanics. Princeton, University Press.

Currey JD, Alexander RM (1985) The thickness of the walls of tubular bones. J Zool 206:453-468

Damilakis J, Maris TG, Karantanas AH (2007) An update on the assessment of osteoporosis using radiologic techniques. Eur Radiol 17:1591-1602

de Margerie E, Sanchez S, et al. (2005) Torsional resistance as a principal component of the structural design of long bones: Comparative multivariate evidence in birds. Anatomical Record Part a - Discoveries in Molecular Cellular and Evolutionary Biology 282A:49-66

Dial KP (1992) Activity patterns of the wing muscles of the pigeon (*Columba livia*) during different modes of flight. J Exp Zool 262:357-373

Dumont ER (2010) Bone density and the lightweight skeletons of birds. Proc R Soc Lond B 277: 2193-2198

Franklin K (1999) Vertical Flight. NAFA Journal 1999:68-72

Franklin K (2011) National Geographic Birds of Prey: High-Velocity Falcons (National Geographic Channel). Available: http://video.nationalgeographic.com/video/.

Habib MB, Ruff CB (2008) The effects of locomotion on the structural characteristics of avian limb bones. Zool J Linn Soc 153:601-624

Heinzel H, Fitter R, Parslow J (1992) Pareys Vogelbuch. Hamburg, Berlin, Paul Parey.

Kalender WA, Felsenberg D, Genant HK, Fischer M, Dequeker J, Reeve J (1995) The European spine phantom — a tool for standardization and quality control in spinal bone mineral measurements by DXA and QCT. European J Radiol 20:83-92

Marshall D, Johnell O, Wedel H (1996) Meta-analysis of how well measures of bone mineral density predict occurrence of osteoporotic fractures. British Med J 312:1254-1259

Mebs T, Schmidt D (2005) Die Greifvögel Europas, Nordafrikas und Vorderasiens. Stuttgart, Kosmos.

Norberg UM (1981) Flight, morphology and the ecological niche in some birds and bats. Symp Zool Soc Lond 48:173-197

Norberg UM (1985). Flying, gliding, and soaring. Functional vertebrate morphology. In: Hildebrand M, Bramble DM, Liem KF, Wake DB (eds). Cambridge, Harvard University Press**,** pp 129-158

Oliver WC, Pharr GM (1992) An improved technique for determining hardness and elastic modulus using load and displacement sensing indentation experiments. J Mater Res 7: 1564-1583

Orton DA (1975). The speed of the peregrine's dive. The Field 25:588-590

Pennycuick CJ (1968) Power requirements for horizontal flight in pigeon *Columba livia*. J Exp Biol 49:527-555

Peter D, Kestenholz M (1998) Sturzflüge von Wanderfalke *Falco peregrinus* und Wüstenfalke *F. pelegrinoides*. Der Ornithologische Beobachter 95:107-112

Ponitz BA, Triep M, Brücker C (2014b). Aerodynamics of the cupped wings during peregrine
    falcon's diving flight. Open J Fluid Dynamics 4:363-372

Ponitz B, Schmitz A, Fischer D, Bleckmann H, Brücker C (2014a) Diving-flight aerodynamics of
    a peregrine falcon (*Falco peregrinus*). Plos One 9:1-13

Purslow PP, Vincent JFV (1978) Mechanical properties of primary feathers from the pigeon. J
    Exp Biol 72:251-260

Rodriguez-Florez N, Oyen ML, Shefelbine SJ (2013) Insight into differences in nanoindentation
    properties of bone. J Mech Behav Biomed Materials 18:90-99

Rubin CT, Lanyon LE (1982) Limb mechanics as a function of speed and gait - a study of
    functional strains in the radius and tibia of horse and dog. J Exp Biol 101:187-211

Ruegsegger P, Elsasser U, Unliker M, Gnehm H, Kind H, Prader A (1976) Quantification of bone
    mineralization using computed tomography. Radiol 121:93-97

Savage C (1992) Peregrine Falcons. San Francisco, Sierra Club.

Schmitz A, Ponitz B, Brücker C, Schmitz H, Herweg J, Bleckmann H (2015) Morphological
    properties of the last primaries, the tail feathers, and the alulae of *Accipiter nisus*,
    Columba livia, *Falco peregrinus* and *Falco tinnunculus*. J Morphol 276:33-46

Seitz K (1999) Vertical flight. NAFA J 38:68-72

Selker F, Carter DR (1989) Scaling of long-bone fracture strength with animal mass. J Biomech
    22: 1175-1183

Simons ELR, Hieronymus TL, O'Connor PM (2011) Cross sectional geometry of the forelimb
    skeleton and flight mode in pelecaniform birds. J Morphol 272:958-971

Swartz SM (1997) Allometric patterning in the limb skeleton of bats: implications for the mechanics and energetics of powered flight. J Morphol 234:277-294

Swartz SM, Bennett MB, Carrier DR (1992) Wing bone stresses in free flying bats and the evolution of skeletal design for flight. Nature 359:726-729

Tang B, Ngan AHW (2004) Investigation of viscoelastic properties of amorphous selenium near glass transition using depth-sensing indentation. Soft Materials 2:125-144

Tang B, Ngan AH, Lu WW (2007) An improved method for the measurement of mechanical properties of bone by nanoindentation. J Mat Sci-Mat Medicine 18:1875-1881

Tucker VA (1990) Body drag, feather drag and interference drag of the mounting strut in a peregrine falcon, *Falco peregrinus*. J Exp Biol 149:449-468

Tucker VA, Parrott GC (1970) Aerodynamics of gliding flight in a falcon and other birds. J Exp Biol 52:345-367

Turner CH, Burr DB (1993) Basic biomechanical measurements of bone - a tutorial. Bone 14: 595-608

Zysset PK, Guo XE, et al. (1999) Elastic modulus and hardness of cortical and trabecular bone lamellae measured by nanoindentation in the human femur. J Biomech 32:1005-1012

Figure legends

Fig. 1 Cross-sections through the humeri of *F. peregrinus* (**a**)*, Columba livia domestica* (**b**)*, F. tinnunculus* (**c**)*, and *A. nisus* (**d**). All humeri are oriented with dorsal side up (dorsal refers to the dorsal side of the wing when fully extended). (**e**) directions of measurement. d dorsal, diag diagonal, lat lateral, v ventral.

Fig. **2** BMD measurements. **a** General set up with the phantom (P) placed directly on the chest of a bird. The gap between the phantom and the animal was reduced to a minimal extent (range 1 to 10 mm depending on species). The picture in **a** shows the transverse image of an entire bird through the breast and wings. Right: thorax of the bird in dorso-ventral and left-lateral view, respectively. Muscles and inner organs are coloured in grey. Example for the measurement of the diaphysis of the ulna of *F. tinnunculus* (**b**) and *F. peregrinus* (**c**)*. The histograms in **d** and **e** show the distribution of the Hounsfield units measured within the region of interest. Size relationships are also indicated. H humerus, Mp M. pectoralis, R radius, U ulna, VC vertebral column, W wing.

Fig. 3 Length and mass of the arm skeleton (**a, b**) and mass of the shoulder skeleton (scapula, coracoid and half of furcula) (**c**) normalized to body mass. Significant differences (P<0.001) are marked by ** (ANOVA, N=8 per species).

Fig. 4 Second moment of area (I) of cross-sections of the humeri (**a**) and specific bending stiffness M calculated for the cross sections (**b**). All data are normalized to body mass. Data are given for (from left to right) the diagonal, lateral and dorso-ventral bending direction (c.f. Fig. 1e). In all cases four animals per species were investigated. Significant differences between *F. peregrinus* and the other species are marked by ** (ANOVA, P<0.001).

Fig. 5 Polar moment of area **J** of the humerus. Polar moment of area (**a**) and polar moment of area normalized to body mass (**b**) for four individuals (2 males and 2 females) of each species (measured in the centre of the humeri). Significant differences are marked by ** (ANOVA, P<0.001).

Fig. 6 Area of the middle humeral cortex (**a**) and the middle humeral cortex normalized to body mass (**b**). Four individuals (2 males and 2 females) per species were investigated. Significant differences are marked by ** (ANOVA, P<0.001).

Fig. 7 K-values of the humeri of the four bird species investigated. Significant differences are marked by ** (ANOVA, P<0.001).

Fig. 8 a Hounsfield units HU (mg cm^{-3}) - measured directly on the bones - on the Hounsfield scale with SD (vertical bars). Values are given for the wing and shoulder skeleton. Significant differences are indicated (P<0.01, ANOVA, post-hoc Bonferroni). **b** HA values for the bones of the wing and shoulder skeleton. HA-values were calculated by using the Hounsfield unit data and calibration data obtained with the phantom.

Fig. 9. Computer aided design model of the cupped wing shape geometry of a peregrine falcon. Contours were generated from multi-view high-resolution camera recordings of a life bird (adult peregrine falcon, mass 500g) in diving motion along a dam wall (c.f. Ponitz et al. 2014a). Note the gap between the inner and outer side of the wing, which allows for aerodynamic side-forces to build up in addition to the lift forces.
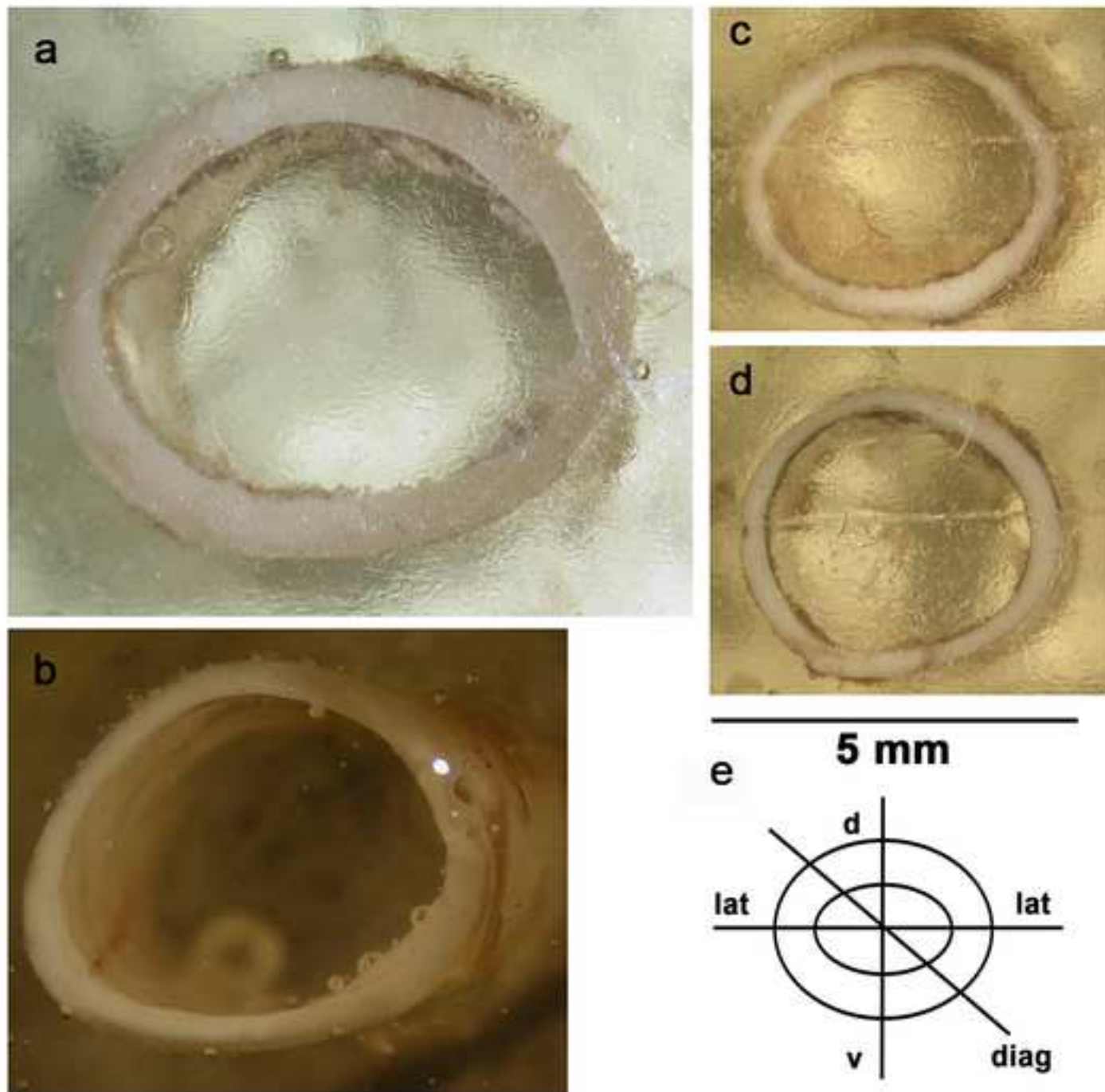
Fig. 10. Isolated forces on the wings for the cupped wing geometry obtained from CFD simulations. Assumed flight speed was 22,5 ms^{-1}, angle of incidence was 5°. The calculated aerodynamic forces are given in a body-related-coordinate-systems (x-direction for caudal, y-direction for dorsal, and z-direction for distal).
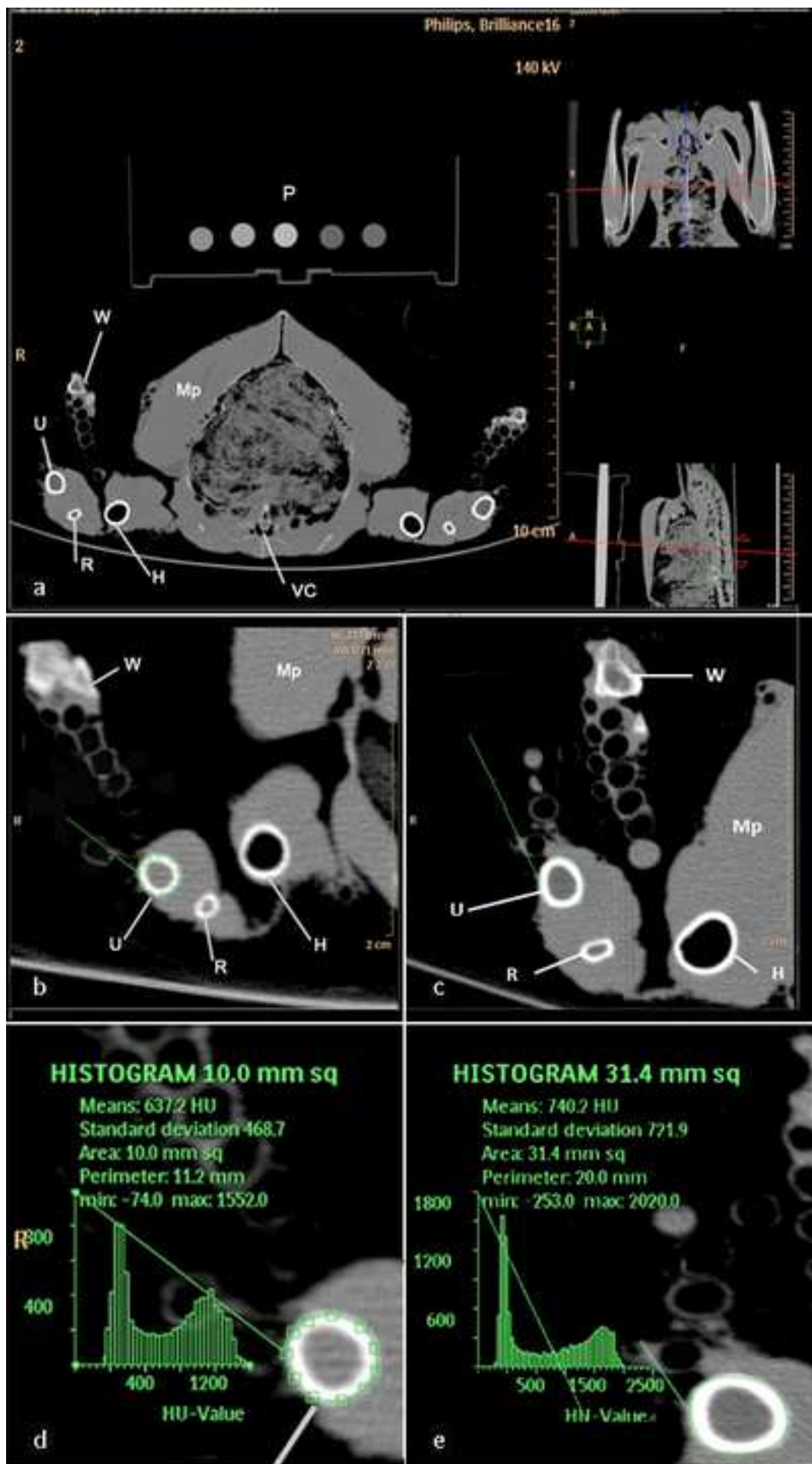
Fig. 11. Scaling of forces with the diving velocity U. For CFD-simulations assumed speeds were 22,5 ms^{-1}, 40 ms^{-1}, and 80 ms^{-1}. The resulting forces are given in a body-related coordinate system (x caudal, y dorsal, and z distal) (c.f. Fig. 10).
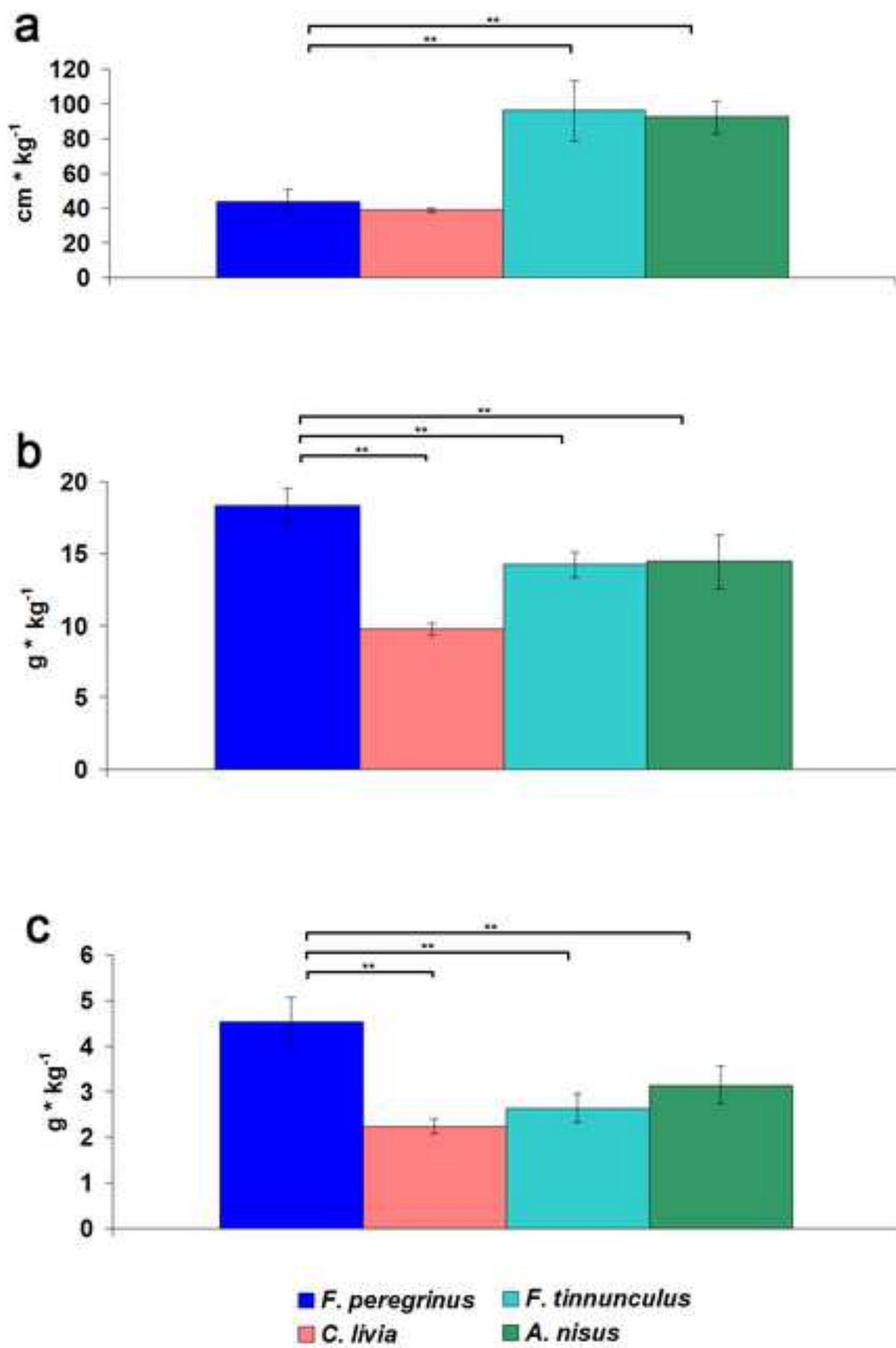
Table 1: Maxima and minima of the second moment of area (I) and Young's modulus E of the humeri of the bird species investigated. Results are given as arithmetic mean (± SD). Significant differences between *F. peregrinus* and the other bird species are marked by * (ANOVA, post-hoc Bonferroni, P<0.01; Mann-Whitney U-test for Young's modulus).
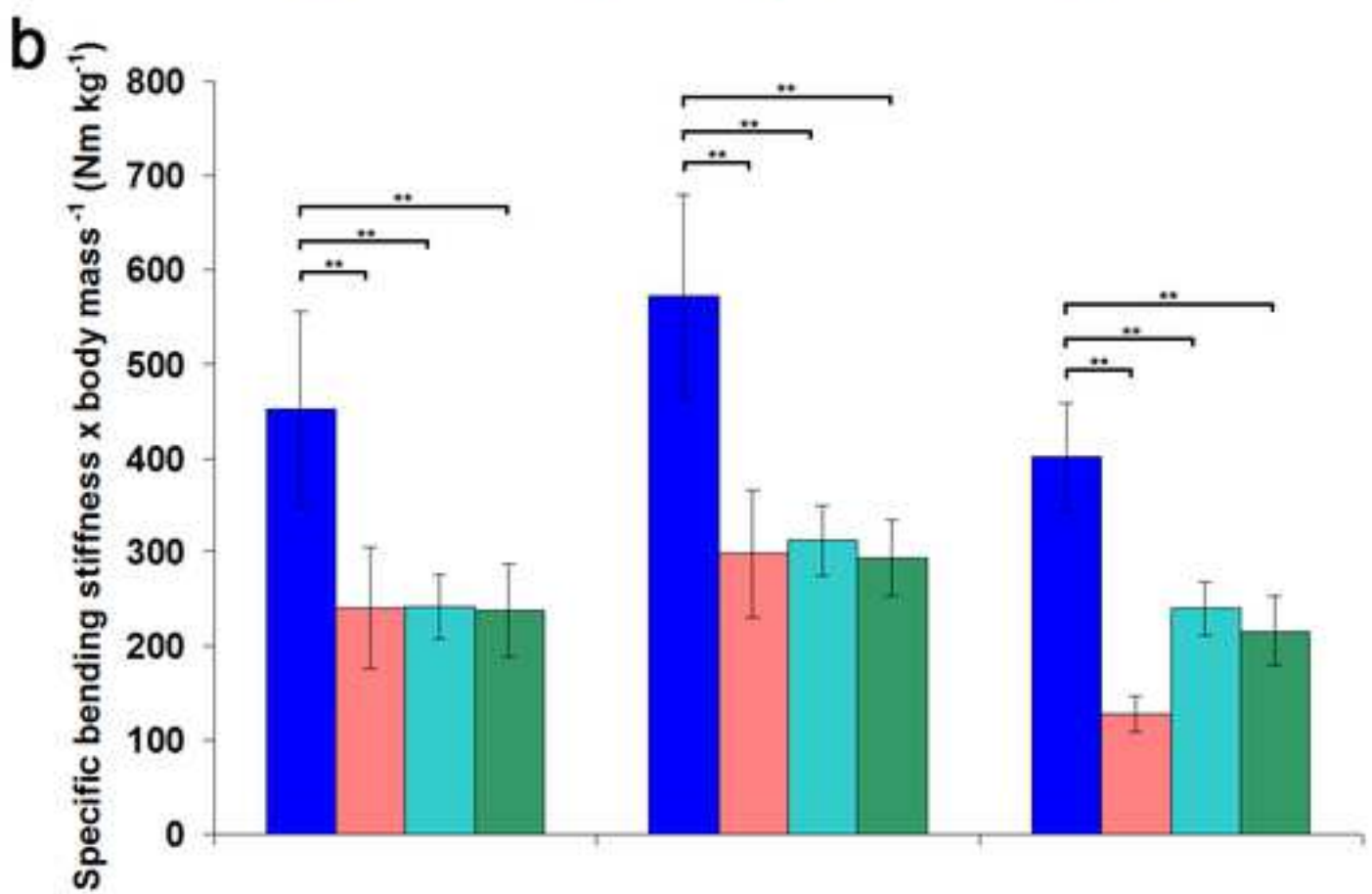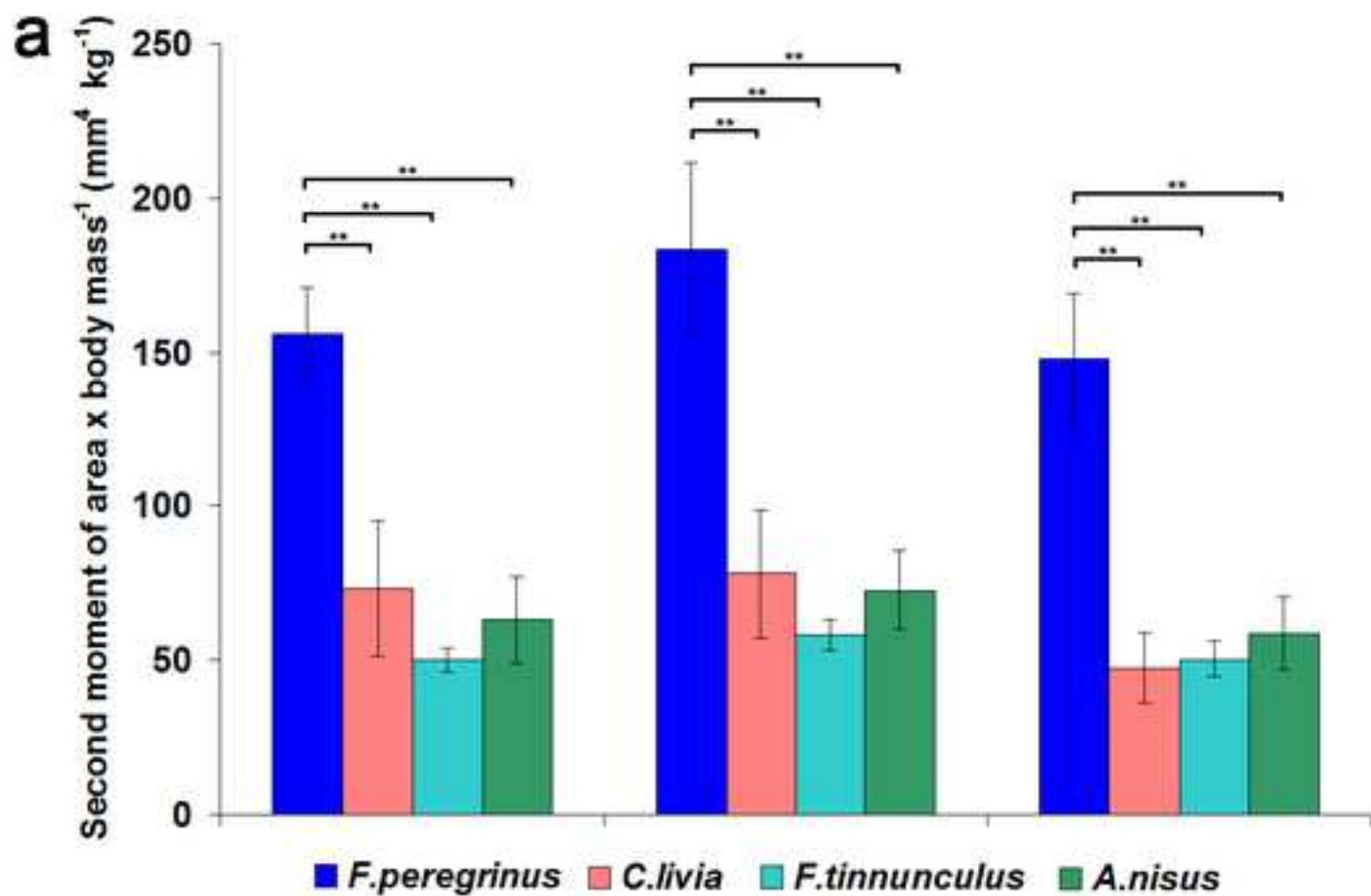
```
 1
 2
 3
 4
 5
 6
 7
 8
 9
10
11
12
13
14
15
16
17
18
19
20
21
22
23
24
25
26
27
28
29
30
31
32
33
34
35
36
37
38
39
40
41
42
43
44
45
46
47
48
49
50
51
52
53
54
55
56
57
58
59
60
61
62
63
64
65
```
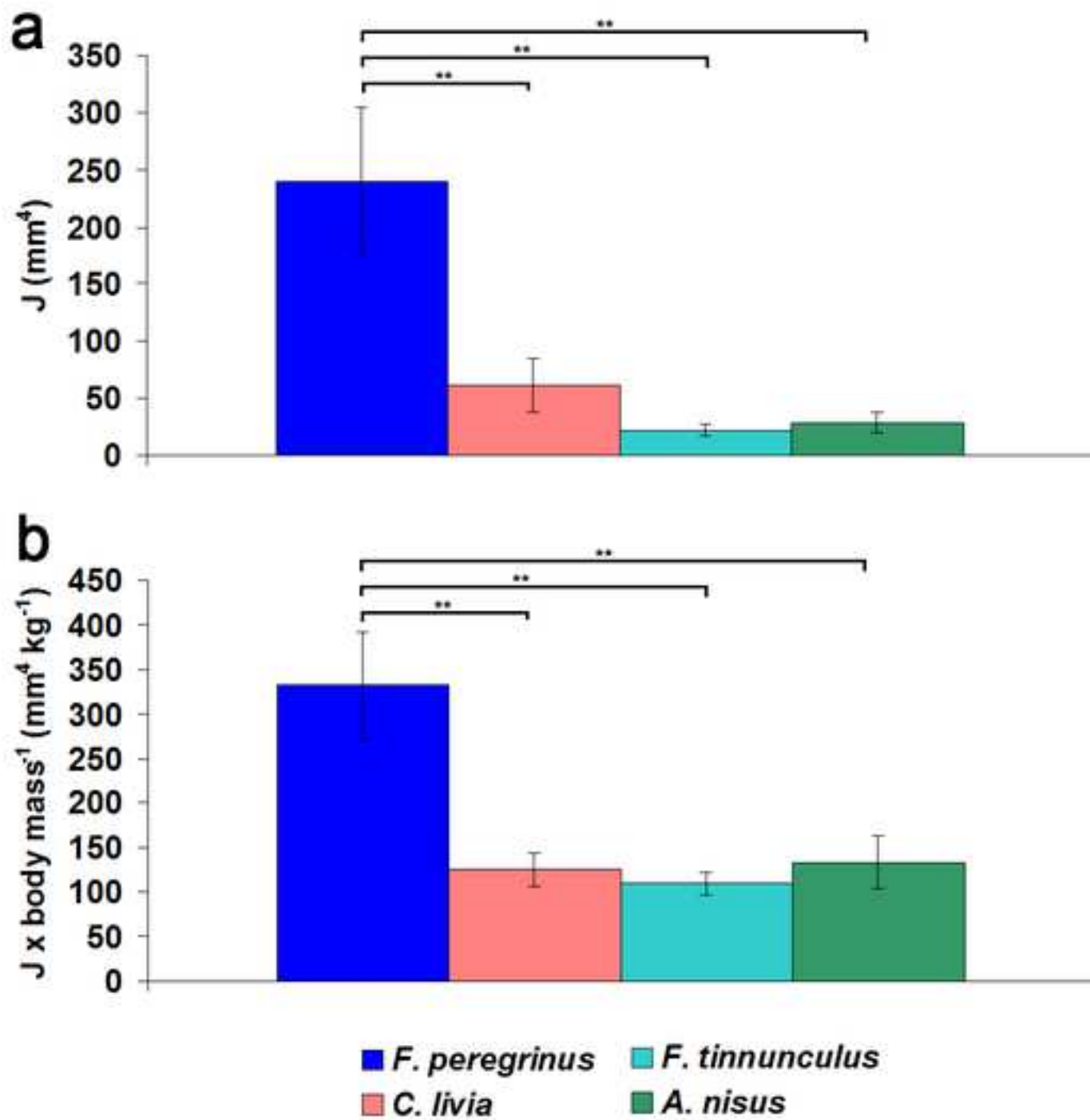
Species	I_{max} (± SD) mm^4	I_{min} (± SD) mm^4	Young's modulus (GPa)
F. peregrinus	132.98 (±35.5)	107.29 (±29.2)	22.7 (±3.9)
C. livia domestica	37.95 (±14.8) *	23.26 (±8.1) *	18.7 (±2.4)
F. tinnunculus	11.76 (±2.27) *	10.21 (±2.15) *	22.6 (±4.3)
A. nisus	15.81 (±5.0) *	12.76 (±4.4) *	19.6 (±3.6)

a

b

c

■ *F. peregrinus*   ■ *F. tinnunculus*
■ *C. livia*   ■ *A. nisus*

a

J (mm⁴) — $J \ (mm^4)$

b

$J \times body \ mass^{-1} \ (mm^4 \ kg^{-1})$

■ *F. peregrinus* ■ *F. tinnunculus*
■ *C. livia* ■ *A. nisus*

$F_Y = 0.90$ N

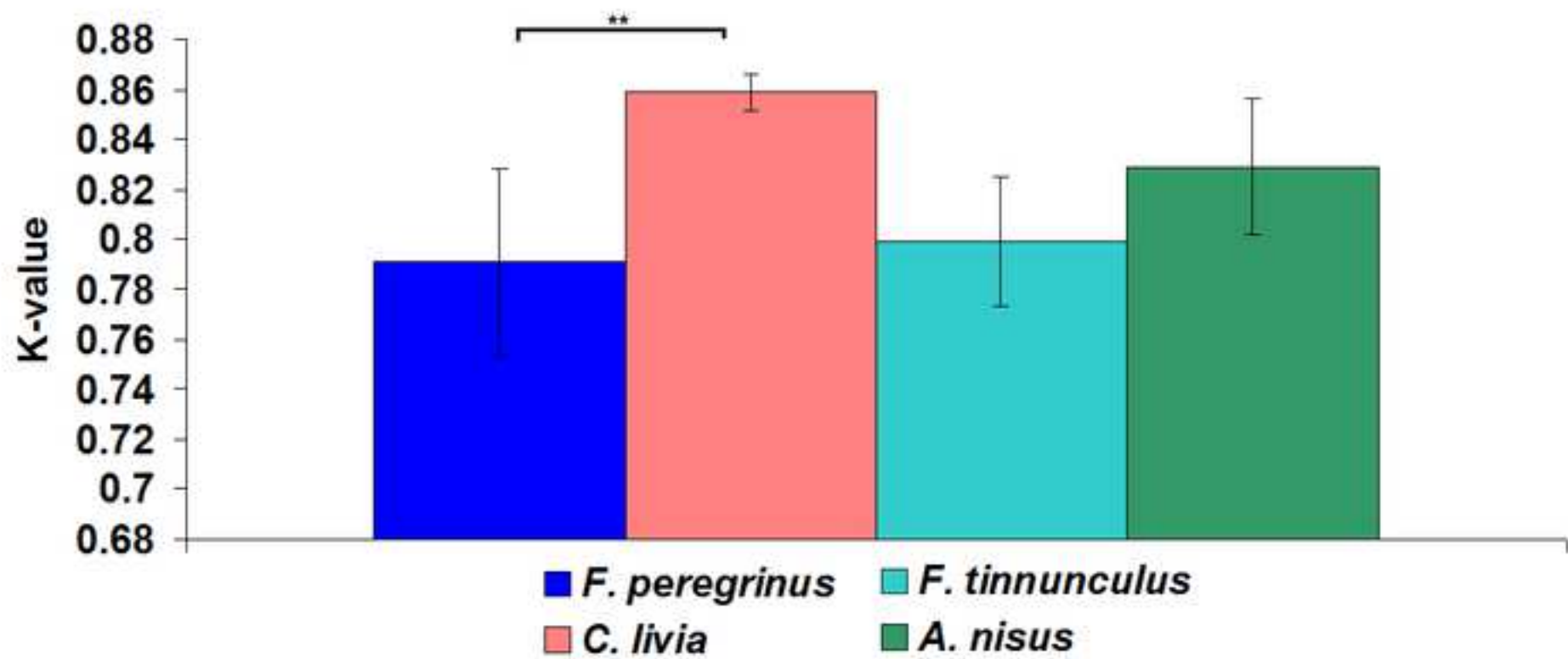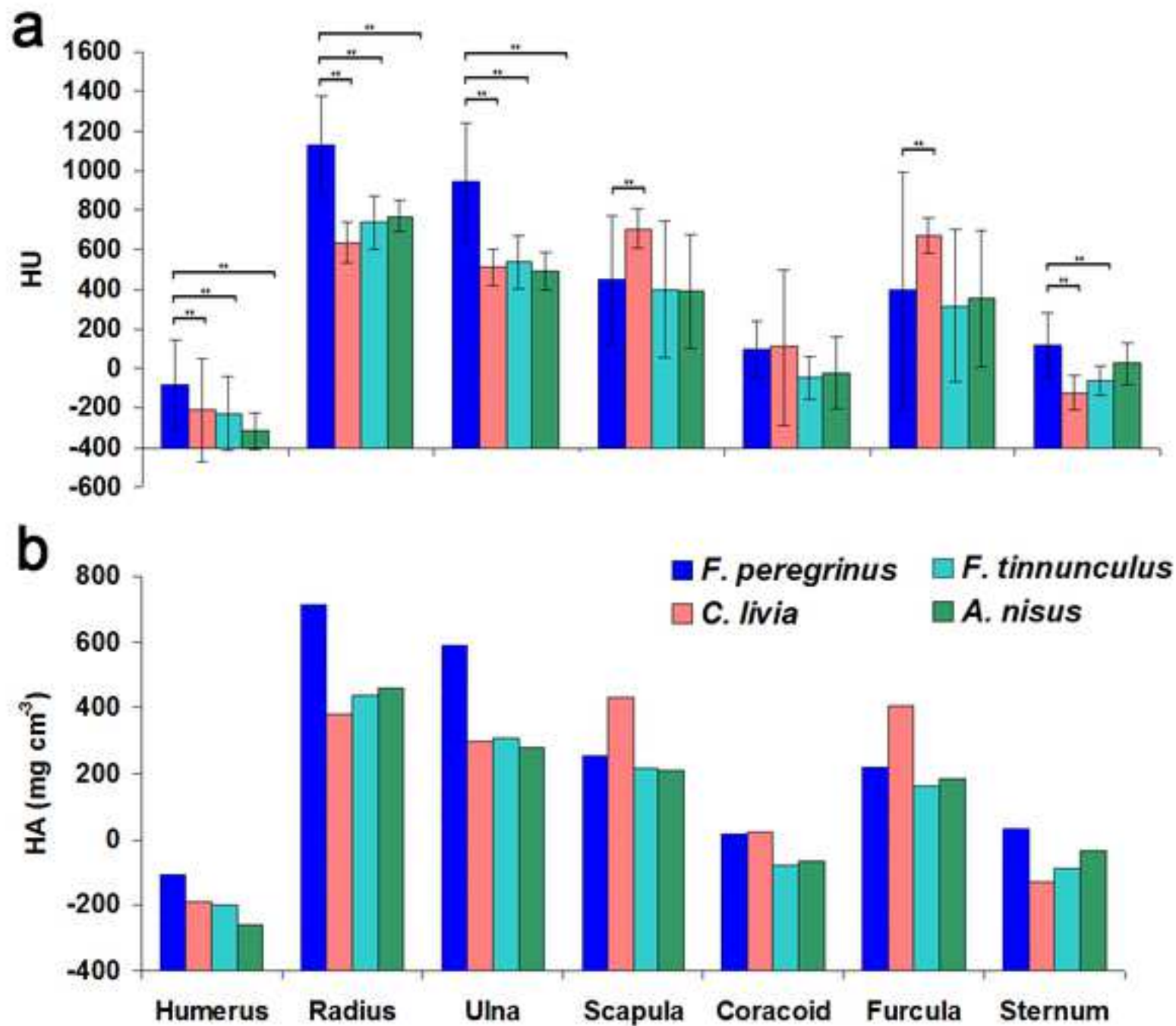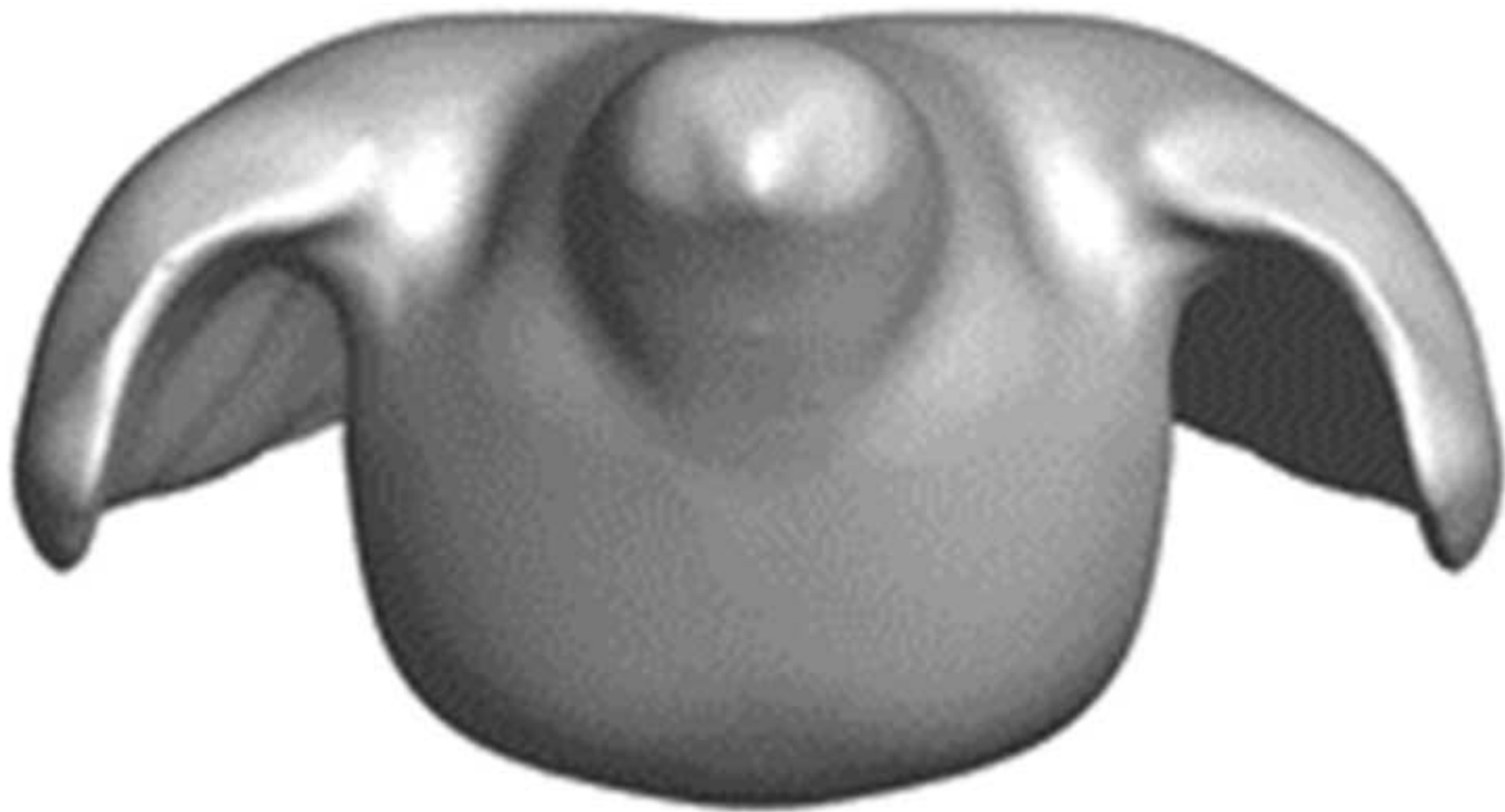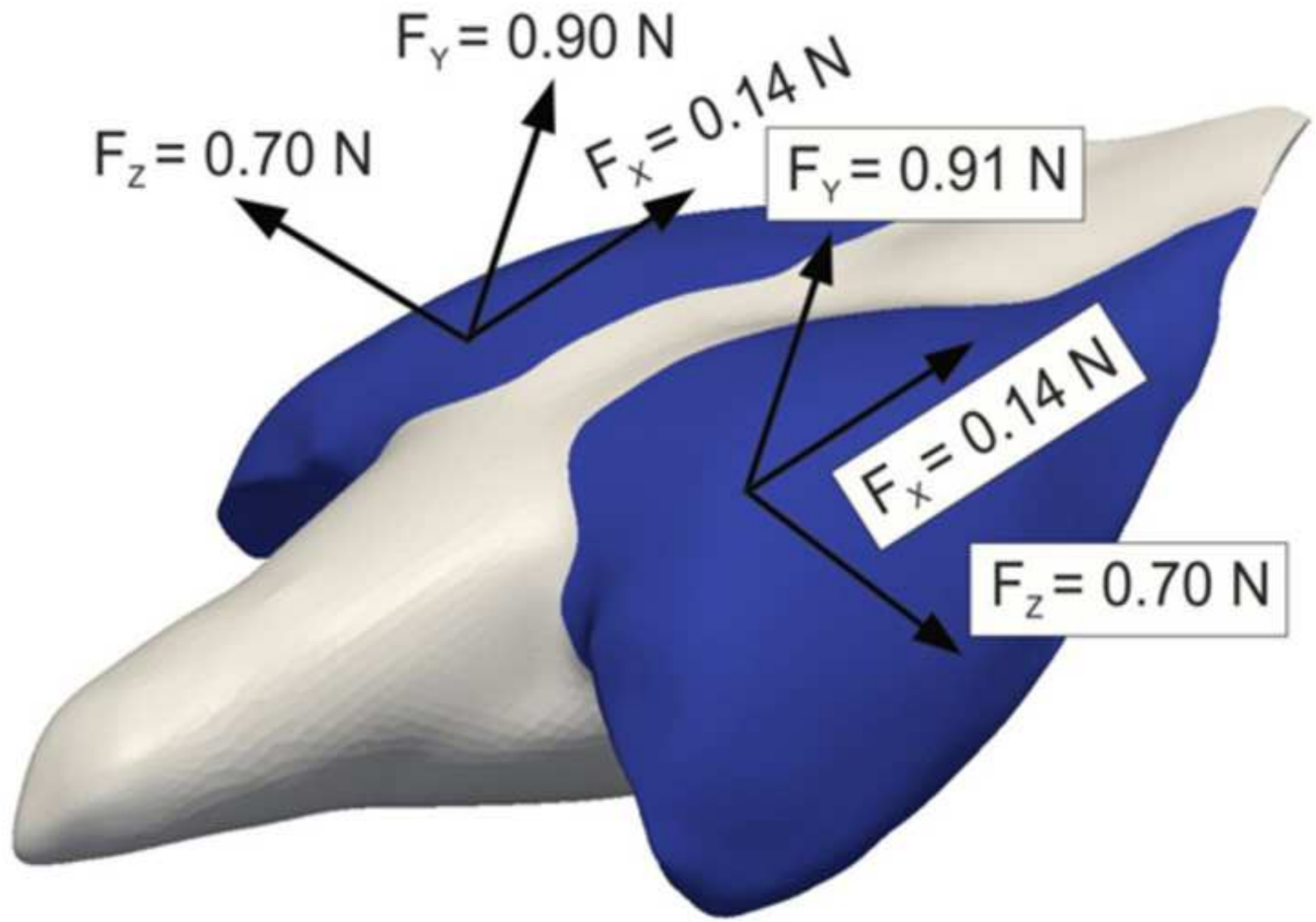$F_X = 0.14$ N

$F_Z = 0.70$ N

$F_Y = 0.91$ N

$F_X = 0.14$ N

$F_Z = 0.70$ N
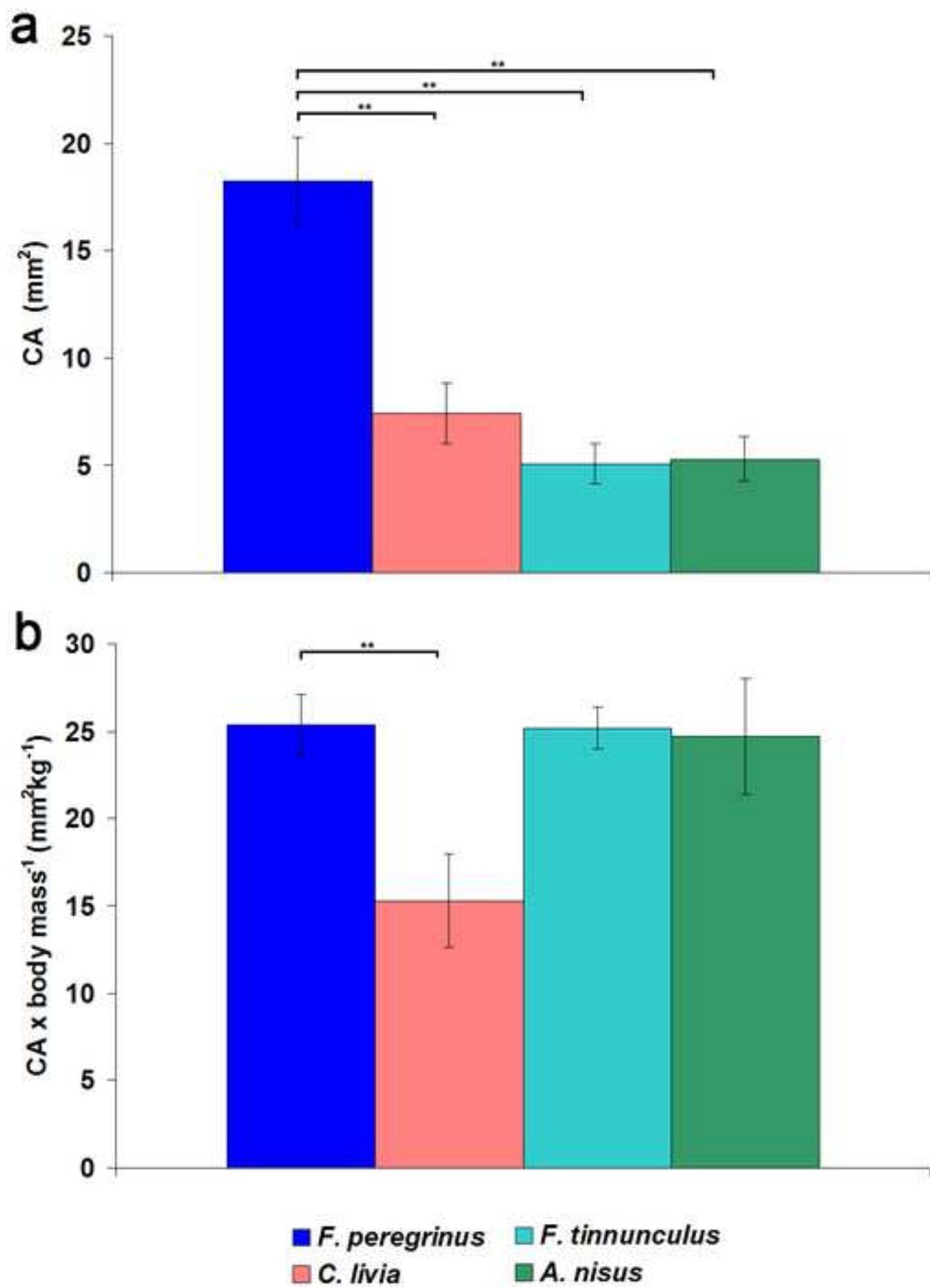
wing forces as a function of speed